scientific reports

OPEN

Adaptive suspension state estimation based on IMMAKF on variable vehicle speed, road roughness grade and sprung mass condition

Xiao Wu[1], Wenku Shi[1], Hong Zhang[2] & Zhiyong Chen[1]✉

Vehicle speed, road roughness grade and sprung mass are the three main factors to influence suspension control and state estimation. Aiming at the problem that fixed state observer cannot guarantee the estimation accuracy of suspension with driving scenario changes, a suspension state observer based on interactive multiple model adaptive Kalman filter (IMMAKF) is established. Firstly, an adaptive control suspension is proposed based on LQR algorithm and multi-objective optimization algorithm, which can automatically adjust the controller parameters according to the vehicle speed, road roughness grade and sprung acceleration parameters, so as to keep the optimal control effect of the suspension. Secondly, the theoretical model of IMMAKF is derived, and two kinds of IMMAKF suspension state observers and controllers are established. Finally, a simulation condition with the vehicle speed, road roughness grade and sprung mass changing simultaneously is established. The simulation results shows that: compared with ordinary IMMKF, AKF and KF observers, the estimation accuracy of IMMAKF5 is improved. Except for state observation, IMMAKF can be used to identify the road roughness grade and estimate the suspension sprung mass.

Suspension is a significant system for vehicles to alleviate road excitation. Active suspension systems use controlled actuator to improve ride comfort and road holding stability[1]. During the control process, the suspension controller needs to get the precise state data through state observer to calculate the optimal controller parameters. The design of controller and state observer is the core of suspension control[2,3].

Ordinary active suspension systems mostly regard state equations as fixed values which are designed by researchers according to the most used working conditions[4]. When the vehicle is driving on special working conditions, the vibration performance like ride comfort is often poor[5,6]. Based on this problem, the adaptive suspension control strategy is proposed[7–9]. Adaptive suspensions can change state equations according to working conditions to optimize the vibration performance. Vehicle longitudinal speed, road roughness grade and sprung mass are the three main factors that affect the vibration performance of suspensions[10]. The calculation of these three factors has a significant impact on the control effect of the suspension. The identification of vehicle longitudinal speed can be divided into direct estimation[11,12] and indirect estimation[13,14]. At the present, with the development of sensors, the use of high-precision onboard speed sensor enables the vehicle to calculate longitudinal speed directly. The estimation of road roughness grade can be divided into two types: vision sensors based measurement[15–17] and state observation based measurement[18–20]. The second method has high accuracy, low cost and good real-time performance. For vehicles, since the total weight of passengers and cargo is random, the value of sprung mass is difficult to calculate. Therefore, the sprung mass is set as a fixed parameter by most current studies[10] or a variable parameter within a certain range. For suspensions with variable sprung mass, the sprung mass is usually set as a state parameter, and the value of sprung mass is estimated by state observation, which is complicated for modeling. Based on this problem, a new suspension controller is proposed to maintain the optimal vibration state of the suspension without calculating the exact value of the sprung mass.

The state equations of adaptive suspensions are changed with the change of working conditions (such as vehicle speed, road roughness grade and sprung mass). If state observers of adaptive suspensions are fixed, the

[1]State Key Laboratory of Automotive Simulation and Control, Jilin University, Changchun, China. [2]Weifang Economic School, Zhucheng, China. ✉email: chen_zy@jlu.edu.cn

precision of state estimation will be low[21,22]. Therefore, fixed state observers are not suitable for the state estimation of adaptive suspensions. The Kalman filter (KF) has high estimation accuracy and low cost, which has been commonly used as observers for vehicle control[23–25] and suspension control[26–30]. In recent years, variable state KF observers are proposed and applied for state estimation of adaptive suspensions, like adaptive Kalman filter (AKF) and interactive multiple model Kalman filter (IMMKF). AKF observer can follow the state of the suspension controller to improve the estimation accuracy. In Ref.[31], suspension sprung acceleration is utilized to identify road roughness grade and determine state equations, then the corresponding AKF is used to estimate the system. In Ref.[32], an adaptive unscented Kalman filter (AUKF) observer is proposed and product-based neural network (PNN) is utilized for road classification. In Ref.[33], a multi-mode switching control strategy of an intelligent suspension system is proposed under different road conditions and the road input is estimated by AKF. IMMKF uses multiple models in parallel for state estimation to reduce observation errors. In Ref.[34], the variable state and road roughness grade are estimated by an interactive multi-model untracked Kalman filter (IMMUKF) observer. The working conditions of the above studies are changing road roughness grade. However, in the actual situation, for adaptive suspensions, the vehicle speed, road roughness grade and sprung mass all have great impacts on system control and state estimation, so just changing the road is not enough to comprehensively improve the suspension performance. For more complex working conditions, AKF and IMMKF have some disadvantages. For AKF, accurate working conditions like road roughness grade and sprung mass should be calculated to switch the observer mode, which is a complicated process. For IMMKF, the number of sub-models increases with the increase of working conditions. If the number of sub-models is too large, the number of parallel computing models is large, which occupies more computer memory and makes program harder.

Based on the idea of changing vehicle speed, road roughness grade and sprung mass simultaneously, IMMAKF observer is proposed for state observation of adaptive suspension. The main contributions of this paper are:

- The IMMAKF suspension state estimation theory is proposed. IMMAKF observer can improve the state estimation accuracy under changing vehicle speed, road grade and sprung mass.
- A new sprung mass estimation theory is proposed. The sprung mass is estimated by model interaction probabilities of IMMAKF without taking it as one of the state parameters to calculate.
- A new adaptive suspension controller system is proposed. The controller system can improve the ride comfort on variable working conditions.

The rest of this paper is organized as follows. Section "Adaptive control suspension model" introduces a new adaptive suspension controller model; Section "Suspension IMMAKF State Estimation Theory" presents the theory of IMMAKF state estimation; Section "Suspension state estimation and control based on IMMAKF" details simulation and comparison and Section "Conclusions" concludes this paper.
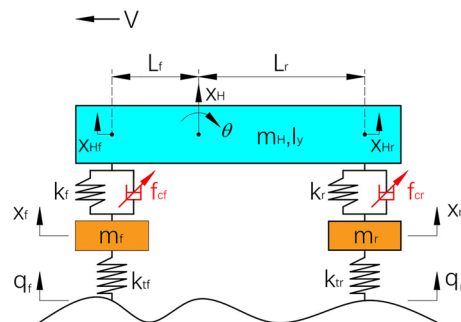
Adaptive control suspension model

In this section, an adaptive control suspension model is established based on LQG and fuzzy control theory to make the vehicle in the optimal state when driving on different working conditions (road roughness grade, vehicle velocity and sprung mass).

LQR Half-car suspension control system modeling

In this part, the half-car suspension system is presented, and the LQR suspension control theory is discussed.

The half-car suspension model is established as Fig. 1. The suspension consists of a spring and an actuator at the front and rear part respectively. The tire is modeled as a linear spring.

Where,m_H denotes the sprung mass;I_y is the pitch inertia;m_f and m_r are front and rear unsprung mass, respectively;k_f,k_r represent front and rear suspension stiffness, respectively;k_{tf},k_{tr} indicate front and rear tire stiffness, respectively;x_H is the sprung mass vertical displacement at the Center of Gravity(CG) point;θ is pitch angle of the sprung mass at the CG point;x_{Hf} and x_{Hr} are the vertical displacement of front and rear sprung mass, respectively;x_f and x_r are the vertical displacement of front and rear unsprung mass, respectively;q_f and

Figure 1. The half-car suspension model.

q_r are the road input at front and rear tire, respectively; f_{cf} and f_{cr} are controlled actuator force at front and rear suspension, respectively; V is the longitudinal vehicle speed.

Parameters of the suspension model are shown in Table 1:

Vertical dynamics equations for the half-car suspension model shown in Fig. 1 can be expressed as:

$$
\begin{aligned}
m_f \ddot{x}_f + k_{tf}(x_f - q_f) + F_f &= 0 \\
m_r \ddot{x}_r + k_{tr}(x_r - q_r) + F_r &= 0 \\
m_H \ddot{x}_H - F_f - F_r &= 0 \\
I_y \ddot{\theta} + L_f F_f - L_r F_r &= 0
\end{aligned}
\tag{1}
$$

where,

$$
\begin{aligned}
F_f &= f_{cf} + k_f(x_f - x_{Hf}) \\
F_r &= f_{cr} + k_r(x_r - x_{Hr})
\end{aligned}
\tag{2}
$$

For the suspension model, and can be approximately calculated as

$$
\begin{aligned}
x_{Hf} &\approx x_H + L_f \theta; \quad \ddot{x}_{Hf} \approx \ddot{x}_H + L_f \ddot{\theta} \\
x_{Hr} &\approx x_H - L_r \theta; \quad \ddot{x}_{Hr} \approx \ddot{x}_H - L_r \ddot{\theta}
\end{aligned}
\tag{3}
$$

Equation (1) can be rewritten as

$$
\mathbf{A}\ddot{\mathbf{x}} + \mathbf{B}\mathbf{x} + \mathbf{C}\mathbf{q} + \mathbf{D}\mathbf{f_c} = \mathbf{0}_{4\times 1}
\tag{4}
$$

where,

$$
\mathbf{q} = \begin{bmatrix} q_f \\ q_r \end{bmatrix}; \mathbf{f_c} = \begin{bmatrix} f_{cf} \\ f_{cr} \end{bmatrix}; \mathbf{A} = \begin{bmatrix} m_H & 0 & 0 & 0 \\ 0 & I_y & 0 & 0 \\ 0 & 0 & m_f & 0 \\ 0 & 0 & 0 & m_r \end{bmatrix}; \mathbf{C} = \begin{bmatrix} 0 & 0 \\ 0 & 0 \\ -k_{tf} & 0 \\ 0 & -k_{tr} \end{bmatrix}; \mathbf{B} = \begin{bmatrix} k_f + k_r & k_f L_f - k_r L_r & -k_f & -k_r \\ k_r L_r - k_f L_f & -k_f L_f^2 - k_r L_r^2 & k_f L_f & -k_r L_r \\ -k_f & -k_f L_f & k_{tf} + k_f & 0 \\ -k_r & k_r L_r & 0 & k_{tr} + k_r \end{bmatrix};
$$

$$
\mathbf{D} = \begin{bmatrix} -1 & -1 \\ L_f & -L_r \\ 1 & 0 \\ 0 & 1 \end{bmatrix} \mathbf{x} = \begin{bmatrix} x_H \\ \theta \\ x_f \\ x_r \end{bmatrix}.
$$

According to[29], q_f and q_r can be calculated as

$$
\begin{aligned}
\dot{q}_f &= -2\pi f_0 q_f + 2\pi n_0 \sqrt{G_q(n_0)V}\,\omega_f \\
\dot{q}_r &= -2\pi f_0 q_r + 2\pi n_0 \sqrt{G_q(n_0)V}\,\omega_r
\end{aligned}
\tag{5}
$$

where, $G_q(n_0)$ is the power spectral density (PSD) of the road profile[35]. f_0 is the lowest cutoff frequency, and $f_0 = 0.01\text{Hz}$[36]. n_0 is the reference spatial frequency, and $n_0 = 0.1\text{m}^{-1}$[37]. ω_f and ω_r denotes zero-mean band-limited white noise.

The road profile is homogeneous and isotropic Gaussian process. The function of road profile[37] is shown as Eq. (6).

$$
G_q(n_k) = G_q(n_0)\left(\frac{n_k}{n_0}\right)^{-W}
\tag{6}
$$

where, n_k is the spatial frequency, W is the road reference coefficient, $W = 2$.

Symbol	Meaning	Unit	Value
m_H	Sprung mass	kg	$300 \sim 500$
I_y	Moment of inertia	kg m^2	$1200 \sim 1500$
m_f	Front unsprung mass	kg	30
m_r	Rear unsprung mass	kg	30
k_f	Front suspension spring stiffness	N m^{-1}	15,000
k_r	Rear suspension spring stiffness	N m^{-1}	15,000
k_{tf}	Front tire stiffness	N m^{-1}	150,000
k_{tr}	Rear tire stiffness	N m^{-1}	150,000
L_f	Distance between mass center to front wheel	m	1.187
L_r	Distance between mass center to front wheel	m	1.533
V	Vehicle velocity	N m^{-1}	$10 \sim 30$

Table 1. Parameters of the half-car suspension model.

According to ISO 8608[38], the road roughness grades are defined from level A to D by $G_q(n_0)(\times 10^{-6} \text{m}^3)$. The range of A grade is [0,32], B is [32,128], C is [128,512] and D is [512,2048]. The road grade corresponding to the geometric mean value of $G_q(n_0)$ in the interval is called ISO standard road. The value of ISO A is 16, ISO B is 64, ISO C is 256 and ISO D is 1024. The ISO standard road is used to as road model in Section "Suspension state estimation and control based on IMMAKF".

According to ISO 8608[38], the road grade index d is defined as:

$$d = \log_2 \left[G_q(n_0) \times 10^6 \right] \tag{7}$$

According to Eq. (7), the road grade is simplified by d. The d of ISO A is 4, ISO B is 6, ISO C is 8, ISO D is 10.

According to Eq. (4) and (5), the state space equations of the half-car suspension system is expressed as Eq. (8).

$$\begin{bmatrix} \ddot{\mathbf{x}} \\ \dot{\mathbf{x}} \\ \dot{\mathbf{q}} \end{bmatrix} = \begin{bmatrix} \mathbf{0}_{4*4} & -\mathbf{A}^{-1}\mathbf{B} & -\mathbf{A}^{-1}\mathbf{C} \\ \mathbf{I}_{4*4} & \mathbf{0}_{4*4} & \mathbf{0}_{4*2} \\ \mathbf{0}_{2*4} & \mathbf{0}_{2*4} & \mathbf{M}_{2*2} \end{bmatrix} \begin{bmatrix} \dot{\mathbf{x}} \\ \mathbf{x} \\ \mathbf{q} \end{bmatrix} + \begin{bmatrix} -\mathbf{A}^{-1}\mathbf{D} \\ \mathbf{0}_{4*2} \\ \mathbf{0}_{2*2} \end{bmatrix} \begin{bmatrix} \mathbf{f_{cf}} \\ \mathbf{f_{cr}} \end{bmatrix} + \begin{bmatrix} \mathbf{0}_{8*2} \\ \mathbf{N}_{2*2} \end{bmatrix} \begin{bmatrix} \omega_{\mathbf{f}} \\ \omega_{\mathbf{r}} \end{bmatrix} \tag{8}$$

Equation (8) is rewritten as

$$\dot{X} = A_0 X + B_0 u + G_0 \omega$$
$$Y = C_0 X + D_0 u \tag{9}$$

where,

$$\mathbf{X} = \begin{bmatrix} \dot{\mathbf{x}} \\ \mathbf{x} \\ \mathbf{q} \end{bmatrix}; \mathbf{u} = \mathbf{f_c} = \begin{bmatrix} \mathbf{f_{cf}} \\ \mathbf{f_{cr}} \end{bmatrix}; \omega = \begin{bmatrix} \omega_{\mathbf{f}} \\ \omega_{\mathbf{r}} \end{bmatrix}; \mathbf{G_0} = \begin{bmatrix} \mathbf{0}_{8*2} \\ \mathbf{N}_{8*2} \end{bmatrix}; \mathbf{q} = \begin{bmatrix} q_f \\ q_r \end{bmatrix}; \mathbf{M} = \begin{bmatrix} -2\pi f_0 & 0 \\ 0 & -2\pi f_0 \end{bmatrix}$$

$$\mathbf{A_0} = \begin{bmatrix} \mathbf{0}_{4*4} & -\mathbf{A}^{-1}\mathbf{B} & -\mathbf{A}^{-1}\mathbf{C} \\ \mathbf{I}_{4*4} & \mathbf{0}_{4*4} & \mathbf{0}_{4*2} \\ \mathbf{0}_{2*4} & \mathbf{0}_{2*4} & \mathbf{M}_{2*2} \end{bmatrix}; \mathbf{B_0} = \begin{bmatrix} -\mathbf{A}^{-1}\mathbf{D} \\ \mathbf{0}_{4*2} \\ \mathbf{0}_{2*2} \end{bmatrix}; \mathbf{N} = \begin{bmatrix} 2\pi\sqrt{G_q(n_0)V} & 0 \\ 0 & 2\pi\sqrt{G_q(n_0)V} \end{bmatrix};$$

$$Y = \begin{bmatrix} \ddot{x}_H & \ddot{\theta} & x_{Hf} - x_f & x_{Hr} - x_r & x_f - q_f & x_r - q_r \end{bmatrix}'$$

To balance the ride comfort and handling stability of the vehicle under variable working conditions, the optimal controllable actuator force f_{cf} and f_{cr} are calculated by LQR algorithm.

The LQR controller is designed as Eq. (10):

$$J = \frac{1}{2} \int_0^\infty J_0 dt = \frac{1}{2} \int_0^\infty \left(X^T Q X + U^T R U + 2 X^T N U \right) dt \tag{10}$$

where J_0 is the suspension comprehensive performance index. J_0 is calculated as Eq. (11).

$$J_0 = q_1(x_{Hf} - x_f)^2 + q_2(\ddot{x}_{Hf})^2 + q_3(x_f - q_f)^2$$
$$+ q_4(x_{Hr} - x_r)^2 + q_5(\ddot{x}_{Hr})^2 + q_6(x_r - q_r)^2 \tag{11}$$

According to Eq. (3), J_0 is calculated as:

$$J_0 = q_1(x_H + L_f\theta - x_f)^2 + q_2(\ddot{x}_H + L_f\ddot{\theta})^2 + q_3(x_f - q_f)^2$$
$$+ q_4(x_H - L_r\theta - x_r)^2 + q_5(\ddot{x}_H - L_r\ddot{\theta})^2 + q_6(x_r - q_r)^2 \tag{12}$$

where, q_1 and q_4 are the controller parameters of suspension deflection of front and rear suspension respectively, q_2 and q_5 are the controller parameters of sprung mass acceleration of front and rear suspension respectively, q_3 and q_6 are the controller parameters of tire deflection of front and rear tire respectively.

The optimal controllable actuator force f_{cf} and f_{cr} are calculated by Eq. (13)

$$f_c = -Kx = -(B^T P + N^T)x \tag{13}$$

where, P is the solution of Riccati equation[20]:

$$PA + A^T P - (PB + N)R^{-1}(B^T P + N^T) + q = 0 \tag{14}$$

When the best controllable actuator force is solved by Eq. (13), the optimal state space equations of LQR half-car suspension system are

$$\dot{x} = A_{LQG}x + B_{LQG}\omega$$
$$y = C_{LQG}x \tag{15}$$

where,

$$A_{LQG} = A - BK$$
$$B_{LQG} = G$$
$$C_{LQG} = C - EK$$

In the actual control process, according to Eq. (15), the system state equations is discretized as Eq. (16).

$$x(k+1) = G_{LQG}x(k) + H_{LQG}\omega(k)$$
$$y(k) = C_{LQG}x(k) + v(k)$$

(16)

where, k is the sampling time, $\omega(k)$ is the process noise, and $v(k)$ is the sampling noise. $\omega(k)$ and $v(k)$ are Gaussian sequences with mean value of 0, and the time interval is 0.01 s.

Multi-objective optimization of suspension controller parameters

In this part, the controller parameters of LQR algorithm (q_1 to q_6) under variable working conditions are optimized by the second non-dominated sorting genetic algorithm (NSGA-II).

For suspension optimal control, the optimization of the suspension controller parameters is regarded as a multi-objective optimization problem (MOOP). The road handling and ride comfort are two conflict properties. It's arduous to get a satisfactory ride comfort without sacrificing the control ability and vice versa. On the other hand, for different working conditions, the optimal LQR controller parameters are different. To keep the best suspension vibration effect under variable working conditions, LQR suspension controller parameters (q_1 to q_6) are optimized by the NSGA-II algorithm. In order to facilitate the optimization process, set $q_1 = q_4, q_2 = q_5, q_3 = q_6$.

Since q_3 and q_6 have little influence on the driving characteristics of suspension, set $q_3 = q_6 = 0.0001$. The optimization process is a MOOP. The optimization decision variables are defined as $q_1(q_4)$ and $q_2(q_5)$. The objective functions, optimization goals and constraints are shown as Eq. (17).

$$\min |\ddot{x}_H|(RMS)$$
$$\min 0.5(\max(|x_{Hf} - x_f|) + \max(|x_{Hr} - x_r|))$$
$$S.T.\max(|x_{Hf} - x_f|) < 0.15$$
$$S.T.\max(|x_{Hr} - x_r|) < 0.15$$
$$S.T.0 \le q_1 \le 10^9$$
$$S.T.0 \le q_2 \le 2000$$

(17)

For NSGA-II optimization, the population size is 30, the number of generations is 100. The vehicle speed is $10 \sim 30$ m s^{-1}(10, 15, 20, 25, 30 m s^{-1}), road roughness grade is A ~ D class (A, B, C and D) and sprung mass is $300 \sim 500$ kg (300, 350, 400, 450, 500 kg). With the combination of these conditions, 100 kinds of different conditions are obtained and optimized by NSGA-II.

The optimization results of vehicle speed 20 m s^{-1}, road grade C and sprung mass 400 kg are shown as Fig. 2c. The q_1 and q_2 of the point that is the closest to the origin of coordinates are selected as the best controller parameters of this condition. The best controller parameters under various working conditions are shown in Fig. 2a,b.

According to Fig. 2a,b, with the increasing of vehicle speed V or road roughness grade index d, or the decreasing of sprung mass m_H, q_1 is decreased and q_2 is increased. This is because with V and d increasing, and m_H decreasing, the sprung mass acceleration $|\ddot{x}_H|$ has an increasing tendency which deteriorates the riding comfort. Based on this, decreasing q_1 and increasing q_2 can improve the suspension deflection (i.e.$|x_{Hf} - x_f|$ and $|x_{Hr} - x_r|$)and reduce the sprung mass acceleration (i.e.$|\ddot{x}_H|$), which can improve the riding comfort.

Adaptive suspension controller modelling

In this part, according to the optimal results of q_1 and q_2 shown in Fig. 2, the fuzzy adaptive suspension controller is proposed and the parameters of the IMMAKF sub-models are calculated.

Based on the optimization results of Fig. 2, the fuzzy adaptive suspension controller model is established. Compared with the vehicle speed V and road grade d, the sprung mass m_H is difficult to be directly measured. Since sprung mass acceleration $\ddot{x}_H$ is influenced by the sprung mass m_H, the fuzzy controller is built with vehicle speed V, road roughness grade index d and sprung mass acceleration $|\ddot{x}_H|$ as inputs, q_1 and q_2 as output respectively.

The fuzzy subset of input variable is divided into: VS (very small), S (small), LS (little small), M (medium), LB (little big), B (big), VB (very big), and the fuzzy subset of output variable is divided into: S1, S2, S3, S4, S5, M, B1, B2, B3, B4, B5. Centroid style is set as fuzzy control mode. The fuzzy control relationships are shown in Fig. 3.

According to Fig. 3, with vehicle speed V, road grade index d and absolute value of vehicle acceleration $|\ddot{x}_H|$ increase, q_1 is decreased and q_2 increased, which makes the body acceleration $\ddot{x}_H$ always be maintained at a small trend to improve the vehicle ride comfort.

The established fuzzy adaptive suspension model is simulated to calculate the parameters of IMMAKF sub-models. As an example, the simulation condition is ISO C road, the vehicle speed is 20 m s^{-1}, the simulation duration is 250 s, and the sprung mass changes as 300–350–400–450-500 kg every 50 s. q_1 and q_2 are extracted in the simulation process, as shown in Fig. 4:

According to Fig. 4, controller parameters are automatically adjusted by the fuzzy adaptive suspension model according to the working conditions. In Fig. 4, the mean value of q_1 and q_2(as shown in the red lines in Fig. 4) are changed with sprung mass m_H.When the sprung mass m_H increases, the mean value of q_1 increases but q_2
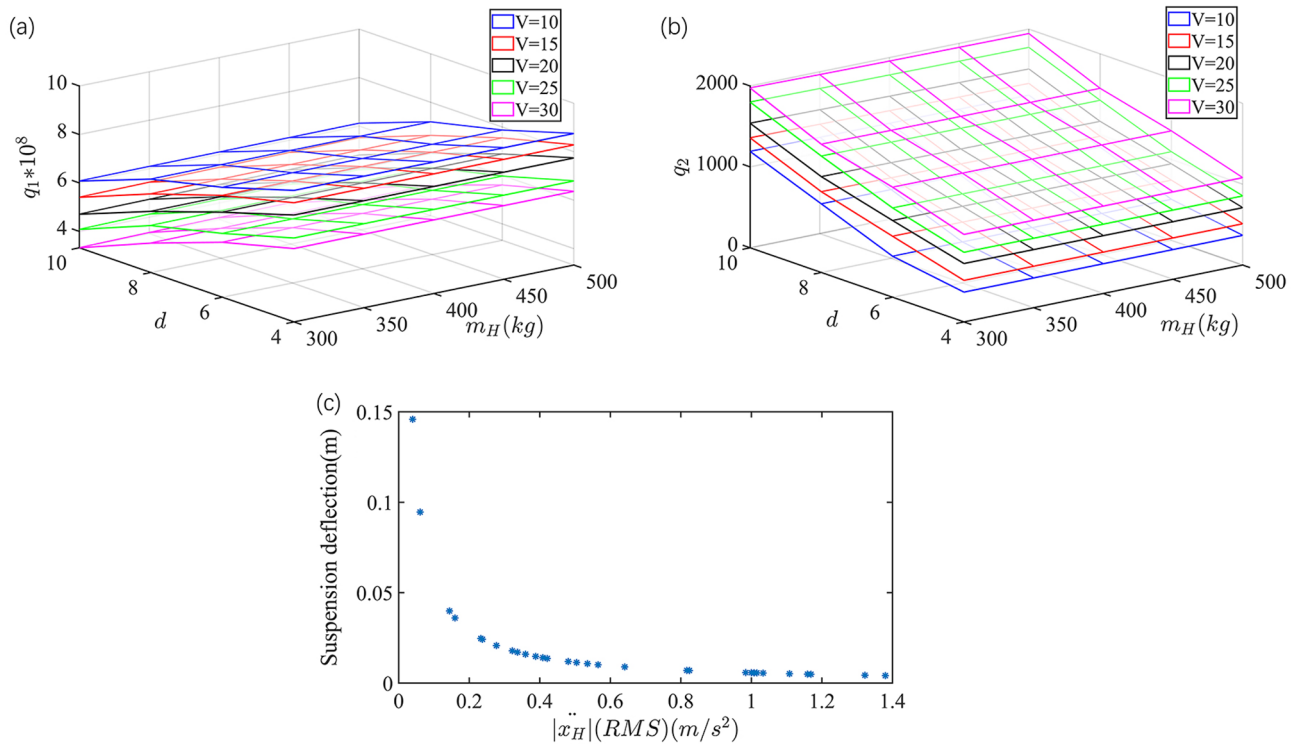
Figure 2. Optimization result of q1 and q2.
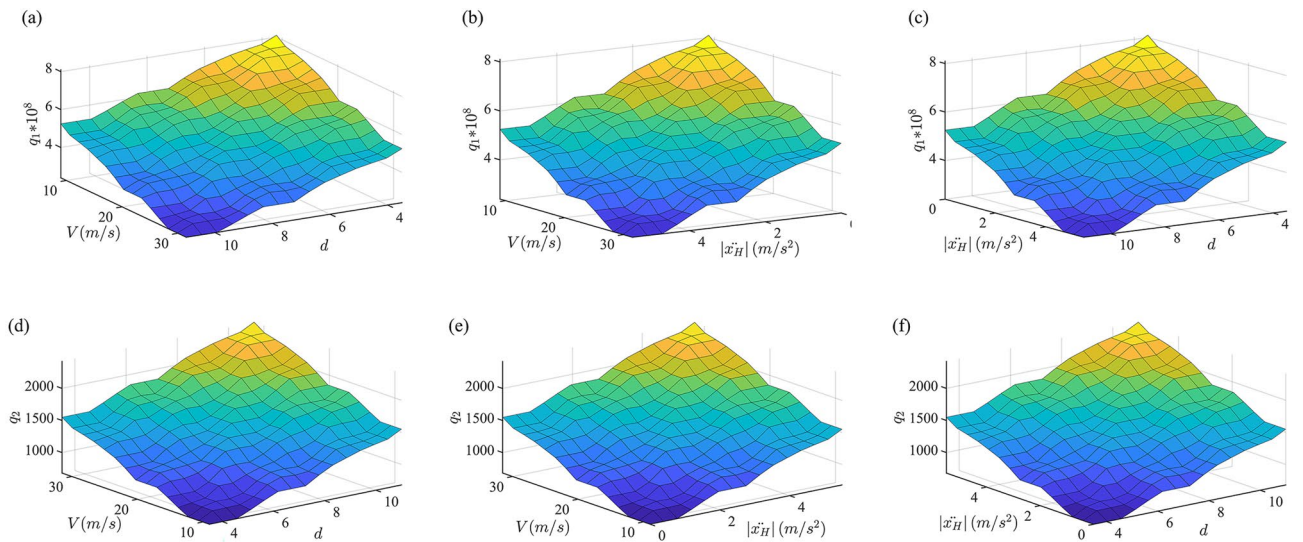
Figure 3. The fuzzy control relationships. (**a, b, c**) the relationship between d, V,$|\ddot{x}_H|$ and q_1; (**d, e, f**) the relationship between d, V,$|\ddot{x}_H|$ and q_2.

decreases. Therefore, the sprung mass m_H is an important factor to affect controller parameters. The mean values of q_1 and q_2 under various working conditions are calculated as parameters of sub-models of the IMMAKF state observer, as shown in Table A.1.

Suspension IMMAKF state estimation theory

In this section, the suspension IMMAKF state estimation and control theory is provided in details.

In practice, the suspension control effect is influenced by external disturbances (like changing road roughness) and parameter uncertainties (like changing vehicle speed and sprung mass). Within these conditions, the vehicle speed can be directly measured by the on-board sensor, however the road roughness grade, sprung mass and suspension state parameters like suspension deflection and sprung mass vertical velocity are hard to be measured directly.
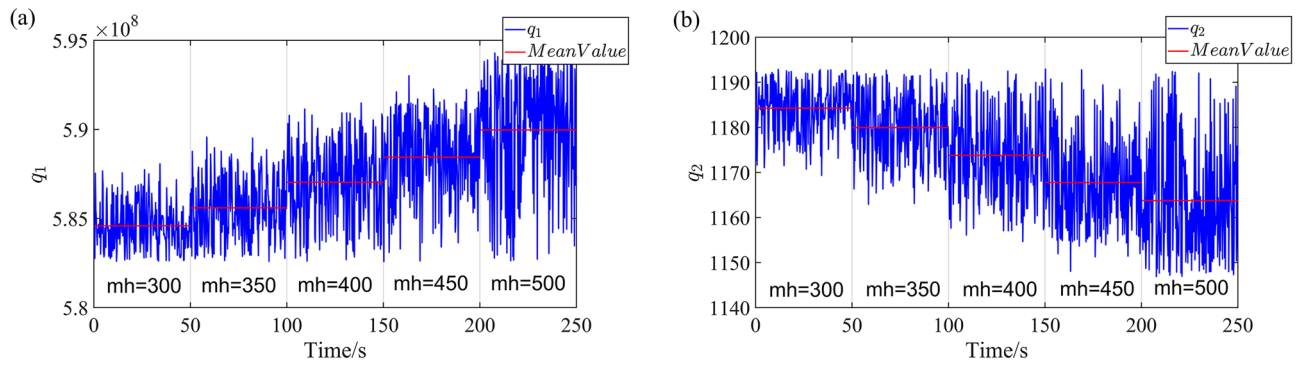
Figure 4. Simulation results of q1 and q2.

The vibration effect of suspension is affected by the estimation precision of each state parameter. At present, Karman Filter (KF) is mostly used as state observer to calculate the real-time state. The ordinary Kalman filter has a high requirement on the accuracy of the system modelling. Since the state of adaptive suspension is changed with the change of working conditions, the ordinary Kalman filter observer is hard to satisfy the high accuracy order of state estimation of adaptive suspensions.

Since the optimal state of the vehicle under various working conditions can be preset (as shown in Table A.1), the suspension state observer of interactive multiple model adaptive Kalman filter (IMMAKF) is proposed by combining adaptive Kalman filter (AKF) and interacting multiple model Kalman filter (IMMKF) to improve the estimation accuracy of adaptive suspension.

State estimation theory of IMMAKF

In this part, the IMMAKF suspension state observer is proposed.

The IMMAKF observer is proposed based on Table A.1. Firstly, the vehicle speed V is determined by the onboard sensor, and the road grade index d is calculated according to the state observation results. Then the adaptive suspension is controlled by the fuzzy control model and the suspension state is estimated by IMMAKF observer. The control and observation process are shown in Fig. 5.

The steps of IMMAKF state estimation are shown as Step 1 to 5.

Step 1: Model interaction.

The IMMAKF state observer is formed with s IMMKF models. Each IMMKF model has r sub-models. All sub-models are Markov processes. Each IMMKF model corresponds to a grade of road, and each IMMKF sub-model corresponds to a sprung mass.

Set $x_{k-1}^{d,i}$ as the original system state of sub-model i of the IMMKF model with road roughness grade index d at the step $t=k$-1, $P_{k-1}^{d,i}$ is the covariance matrix, and $\mu_{k-1}^{d,i}$ is the probability of model i.

After model interaction, the initial conditions of IMMAKF are $x_{k-1}^{d,i,0}$ and $P_{k-1}^{d,i,0}$, and can be calculated as shown in Eq. (18) and (19), respectively.
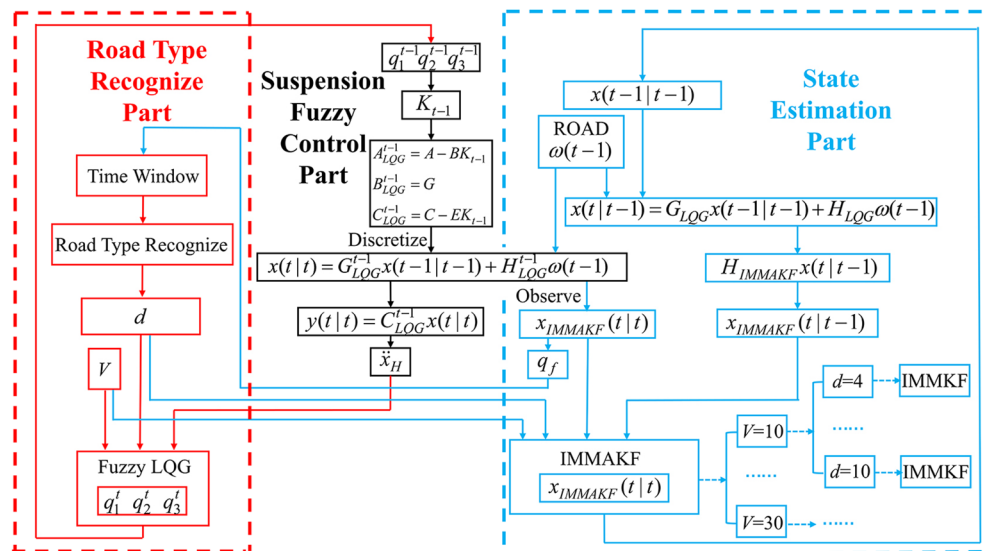
Figure 5. Flow chart of observation and control of IMMAKF.

$$x_{k-1}^{d,i,0} = \sum_{j=1}^{r} x_{k-1}^{d,j} \mu_{k-1}^{d,ji} \tag{18}$$

$$P_{k-1}^{d,i,0} = \sum_{j=1}^{r} \mu_{k-1}^{d,ji} \left[P_{k-1}^{d,j} + (x_{k-1}^{d,j} - x_{k-1}^{d,i,0}) \left(x_{k-1}^{d,j} - x_{k-1}^{d,i,0} \right)^T \right] \tag{19}$$

where

$$\mu_{k-1}^{d,ji} = \frac{p_{ji}^d \mu_{k-1}^{d,j}}{\sum p_{ji}^d \mu_{k-1}^{d,j}} \tag{20}$$

In Eq. (20), $\mu_{k-1}^{d,ji}$ is the mix probability of model j transferred to model i of the IMMKF model with road grade index d at the step $t = k$-1, and p_{ji}^d is the transition probability matrix from model j to model i.

Step 2: Kalman filter.

$x_{k-1}^{d,i,0}$ and $P_{k-1}^{d,i,0}$ calculated in the Step 1 are used for state prediction and prior covariance estimation.

State prediction equation is shown as Eq. (21).

$$x_{k|k-1}^{d,i} = A_i^d x_{k-1}^{d,i,0} + B_i^d u_{k-1}^d \tag{21}$$

Prior covariance equation is shown as Eq. (22).

$$P_{k|k-1}^{d,i} = A_i^d P_{k-1}^{d,i,0} (A_i^d)^T + Q_i^d \tag{22}$$

where, A_i^d and B_i^d are the state equation of model i, and Q_i^d is the process noise variance matrix.

Then the Kalman gain equation $K_k^{d,i}$ is calculated as:

$$K_k^{d,i} = \frac{P_{k|k-1}^{d,i} H^T}{H P_{k|k-1}^{d,i} H^T + R} \tag{23}$$

where, H is the system observation matrix, and R is the measurement noise covariance matrix.

The Kalman filter state is calculated as:

$$x_k^{d,i} = x_{k|k-1}^{d,i} + K_k^{d,i} (Z_k^d - H x_{k|k-1}^{d,i}) \tag{24}$$

where, Z_k^d is the estimation value at the step $t = k$.

The Kalman filter covariance is calculated as:

$$P_k^{d,i} = \left(I - K_k^{d,i} H \right) P_{k|k-1}^{d,i} \tag{25}$$

Step 3: Update model probability.

The observer model is updated by maximum likelihood estimation. By calculating the similarity between the current model and the current target state, the most suitable weight of the current tracking model is given at step $t = k$. The most matched maximum likelihood function of model i is calculated as follows:

$$\Lambda_k^{d,i} = \frac{1}{\sqrt{2\pi^N \det \left| S_k^{d,i} \right|}} \exp\left[-0.5(d_k^{d,i})^T (S_k^{d,i})^{-1} (d_k^{d,i}) \right] \tag{26}$$

where

$$d_k^{d,i} = z_k - H_i x_{k|k-1}^{d,i} \tag{27}$$

$$d_k^{d,i} = z_k - H_i x_{k|k-1}^{d,i} \tag{28}$$

The probability of model i is updated as:

$$\mu_k^{d,i} = \frac{1}{c} \Lambda_k^{d,i} \sum p_{ji}^d \mu_{k-1}^{d,j} \tag{29}$$

where

$$c = \frac{\Lambda_k^{d,i}}{\sum \Lambda_k^{d,i}} \sum p_{ji}^d \mu_{k-1}^{d,j} \tag{30}$$

Step 4: Combine model data.

The results of overall state estimation and overall covariance estimation are calculated by Kalman filter states, Kalman filter covariance and updated probability.

Overall state estimation is calculated as Eq. (31).

$$x_k^d = \sum_{i=1}^{r} x_k^{d,i} \mu_k^{d,i} \tag{31}$$

Overall covariance estimation is calculated as Eq. (32).

$$P_k^d = \sum_{i=1}^{r} \mu_k^{d,i} \left[P_k^{d,i} + \left(x_k^{d,i} - x_k^d \right) \left(x_k^{d,i} - x_k^d \right)^T \right] \tag{32}$$

The model d of Eqs. (18) to (32) is determined by the state estimation of the road profile (i.e.q_f and q_r).

From Step 4, the state parameters are calculated by IMMAKF observer. The road roughness grade is calculated by Step 5.

Step 5: Determine the current road roughness grade.

The road grade index d is calculated by the power spectral density (PSD) of q_f and q_r through state observation, as the reference of mode switching for suspension controller and observer. In this paper, road roughness grade is calculated by q_f. The road displacement unevenness $q(l)$ is calculated by q_f and driving length l. Since sampling time and vehicle speed V are fixed, $q(l)$ can be transformed into $q(n)$.

The average power of $q(n)$ is:

$$P = \frac{1}{N} \sum_{n=0}^{N-1} |q(n)|^2 \tag{33}$$

where N is the total number of points in a sampling process.

From the discrete Fourier transform:

$$Q_m = \sum_{n}^{N-1} q(n) e^{-jmn\frac{2\pi}{N}} \tag{34}$$

According to Parseval theory[31]:

$$\sum_{n=0}^{N-1} |q(n)|^2 = \frac{1}{N} \sum_{m=0}^{N-1} |Q_m|^2 \tag{35}$$

Then Eq. (33) can be expressed as:

$$P = \frac{1}{N^2} \sum_{m=0}^{N-1} |Q_m|^2 \tag{36}$$

Therefore, the power spectral density of $q(n)$ is:

$$P_m = \frac{1}{N} |Q_m|^2 \frac{N}{f_s} = \frac{1}{f_s} |Q_m|^2 \tag{37}$$

where, f_s is the sampling frequency.

By comparing the calculated P_m with standard road roughness grade[32], the grade of the road can be calculated.

The above steps can be iterated to complete the suspension state observation based on IMMAKF. The specific details of IMMAKF state observation can be described as: IMMKF sub-models with different sprung mass acceleration under various vehicle speed and road grade are combined as IMMAKF observer. When the working condition is changed, the suspension controller switches the state according to the speed, road grade and sprung mass acceleration, and then the IMMAKF observer selects the sub-model (IMMKF) according to the state of the controller system. For IMMAKF, the state of observer is always consistent with the state of the suspension controller.

Q and R of IMMAKF state observer

The noise generated in state transition is measured by the process noise variance matrix Q. Q is calculated as Eq. (38).

$$Q = H_{LQG} Q_{RV} Q_{RV}^T B_{LQG}^T \tag{38}$$

where, Q_{RV} is the noise of input road speed, which can be calculated by approximate statistics in Eq. (39).

$$Q_{RV} = \frac{1}{n} \sum_{i=1}^{n} \dot{q}_i \tag{39}$$

where, $\dot{q}_i$ is the input road speed at sampling point i.

The relationship between Q_{RV} and road roughness grade index d described in three degrees polynomial function is:

$$Q_{RV} = 0.00138d^3 - 0.01516d^2 + 0.07753d - 0.08562 \tag{40}$$

The SSE of the fitting function is 7.634×10^{-4}, and the R-square is 0.9992. The fitting accuracy is high.

The noise in the observation process is calculated by the measurement noise covariance matrix R. Set measurement vector as:

$$x_{IMMAKF} = \begin{bmatrix} \dot{x}_H & \dot{\theta} & \dot{x}_f & \dot{x}_r \end{bmatrix}'$$

The observation matrix is:

$$H_{IMMAKF} = \begin{bmatrix} 1 & 0 & 0 & 0 & ... & 0 \\ 0 & 1 & 0 & 0 & ... & 0 \\ 0 & 0 & 1 & 0 & ... & 0 \\ 0 & 0 & 0 & 1 & ... & 0 \end{bmatrix} \tag{41}$$

The size of H_{IMMAKF} is 4×9.

R is dependent on the sensor accuracy and road conditions. According to[33], set $R = 0.01^2$.

Suspension state estimation and control based on IMMAKF

In this section, two IMMAKF observers are established. A variable working condition is established based on changing vehicle speed, road roughness grade and sprung mass. Compared with other Kalman filter observers, the precision of IMMAKF observer is verified by simulation and experiment.

Simulation condition

In practice, the actual working conditions such as vehicle speed, road roughness grade and sprung mass can be changed simultaneously. Based on variable working conditions, referring to Table A.1, the simulation model is established as shown in Fig. 6:

IMMAKF observer models

Two kinds of IMMAKF observers are proposed by Table A.1.

Five-model IMMAKF observer (IMMAKF5): All the data in Table A.1 are selected as the sub-model of IMMAKF observer. Sub-models of IMMAKF5 cover all working conditions and the observation accuracy is high.

Three-model IMMAKF observer (IMMAKF3): the control parameters with sprung masses of 300, 400 and 500 (kg) in Table A.1 are extracted respectively as sub-models of IMMAKF3 observer. Sub-models of IMMAKF3 cover three main working conditions to maintain observation accuracy.

For comparison, data are selected from Table A.1 as other observers: ordinary Kalman filter (KF), AKF and IMMKF. Among them, the results of 20 m s^{-1} vehicle speed, ISO C road and 400 kg sprung mass in Table A.1 are selected as the KF. The results of 20 m s^{-1} vehicle speed, 400 kg sprung mass and all grades of roads are selected as AKF (i.e. for AKF, the vehicle speed and sprung mass are fixed, but road grade can be changed). The results of 20 m s^{-1} vehicle speed, ISO C road and all of the sprung mass are selected as IMMKF (i.e. for IMMKF, the
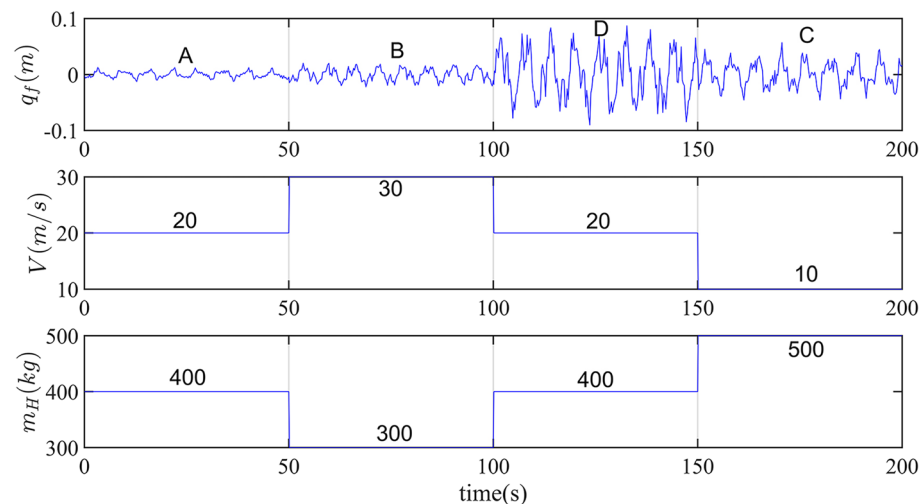
Figure 6. Suspension simulation condition. 0-50 s, V = 20 m s^{-1}, $m_H = 400$kg, ISO A road; 50-100 s, V = 30 m s^{-1}, $m_H = 300$kg, ISO B road; 100-150 s, V = 20 m s^{-1}, $m_H = 400$kg, ISO D road; 150-200 s, V = 10 m s^{-1}, $m_H = 500$kg, ISO C road.

vehicle speed and the road grade are fixed, but the sprung mass is used as the interacting multiple model for state estimation).

Road roughness grade recognition time window

Based on Eq. (33) to Eq. (37), the accuracy of road grade identification is influenced by the number of sampling points. The spatial frequency of road roughness is between $[0.011, 2.83]\text{m}^{-1}$. The minimum identification frequency dn is calculated as Eq. (42).

$$dn = \frac{1}{l} \le 0.011 \tag{42}$$

Then,$l \ge 91\text{m}$.

The minimum identification sampling step number is set as $n_{\min}$, then

$$n_{\min} \; \Delta t \; V_{\min} \ge 91\text{m} \tag{43}$$

where,Δt is sampling interval time of adjacent sampling points, and V is vehicle speed. In this paper, $\Delta t = 0.01s$ and $V_{\min} = 10\text{m/s}$,then $n_{\min} \ge 910$.

The road grade roughness shown in Fig. 6 is estimated by IMMAKF5. Set n as the step number of road roughness grade recognition window. Different road grade estimation accuracy of different n is shown as Table 2.

In Table 2, the higher the number of sampling steps n, the higher the accuracy of road grade recognition, but the longer the distance for the vehicle to derive. Based on the accuracy and the driving time, the step number of road roughness grade recognition window is selected as 1250.

Comparison of simulation results

The IMMAKF5, IMMAKF3, KF, AKF and IMMKF observers are applied to the state estimation of adaptive suspension. The initial road roughness grade of IMMAKF and AKF is determined as A grade (i.e. the initial $d = 4$). The comparison results are shown in Fig. 7:

According to Fig. 7, for all working conditions, the estimation results of IMMAKF5 is the closest to real results, followed by IMMAKF3. Since state equations of adaptive suspensions are changed with the change of vehicle speed, road roughness grade and sprung mass, the state estimation accuracy of fixed state observer is low. Therefore, in Fig. 7, the estimation accuracy of KF is the worst. Compared with KF, both AKF and IMMKF can partly follow the current suspension state (i.e. road grade and sprung mass), which makes the estimation accuracy of AKF and IMMKF lower than IMMAKF but higher than KF.

The simulation error of each observer is calculated as shown in Eq. (44).

$$E_s = \frac{1}{n} \sum_{1}^{n} \frac{|x_{ireal} - x_{iobs}|}{|x_{ireal}|} \times 100\% \tag{44}$$

where, E_s is the simulation error, x_{ireal} is the real value of x_i, x_{iobs} is the observation value of x_i, n is the total number of the sampling points in the simulation, and i is the number of coefficients of state vector x.

The simulation errors of each coefficient of state vector x are shown in Table 3.

Where, IMMAKF5 is results of five-model IMMAKF observer, IMMAKF3 is results of three-model IMMAKF observer. Total is the whole simulation condition. Grade A is the simulation condition of grade A road in Fig. 6.

In Table 3, compared with other observers, the estimation error of IMMAKF3 and IMMAKF5 observers are the smallest. Within the two IMMAKF observers, IMMAKF5 has the highest accuracy. Among the four measurement vector coefficients ($\begin{bmatrix} \dot{x}_H & \dot{\theta} & \dot{x}_f & \dot{x}_r \end{bmatrix}'$), for the whole simulation process, compared with IMMKF, AKF and KF, the estimation error of $\dot{x}_H$ in IMMAKF5 is reduced by 55.17%, 56.84% and 60.19% respectively; $\dot{\theta}$ is reduced by 48.69%, 48.85% and 45.31% respectively; $\dot{x}_f$ is reduced by 77.18%, 77.43% and 79.36% respectively;$\dot{x}_r$ is reduced by 76.78%, 77.05% and 79.43% respectively. The trend of simulation results on each grade of road is similar to the total simulation process. For other state coefficients, the accuracy of the two IMMAKF observers is also better than other observers, which verifies the superiority of the IMMAKF observer in complex working conditions.

During the simulation, the road grade is calculated by IMMAKF observer. The road grade recognition results for IMMAKF5 and IMMAKF3 are shown in Fig. 8:

In Fig. 8, the road roughness grade recognition results always lag behind the real road in time domain, and the lag time is just the length of a time window. Since the road grade recognition depends on sampling of $q(l)$, the system can't immediately calculate the road grade.

| Sampling step n	ISO A/%	ISO B/%	ISO D/%	ISO C/%
910	85.00	85.00	80.00	85.00
1000	85.00	85.00	87.50	90.00
1100	90.00	90.00	90.00	100.00
1200	100.00	100.00	95.00	100.00
1250	100.00	100.00	100.00	100.00

Table 2. Road grade estimation accuracy.
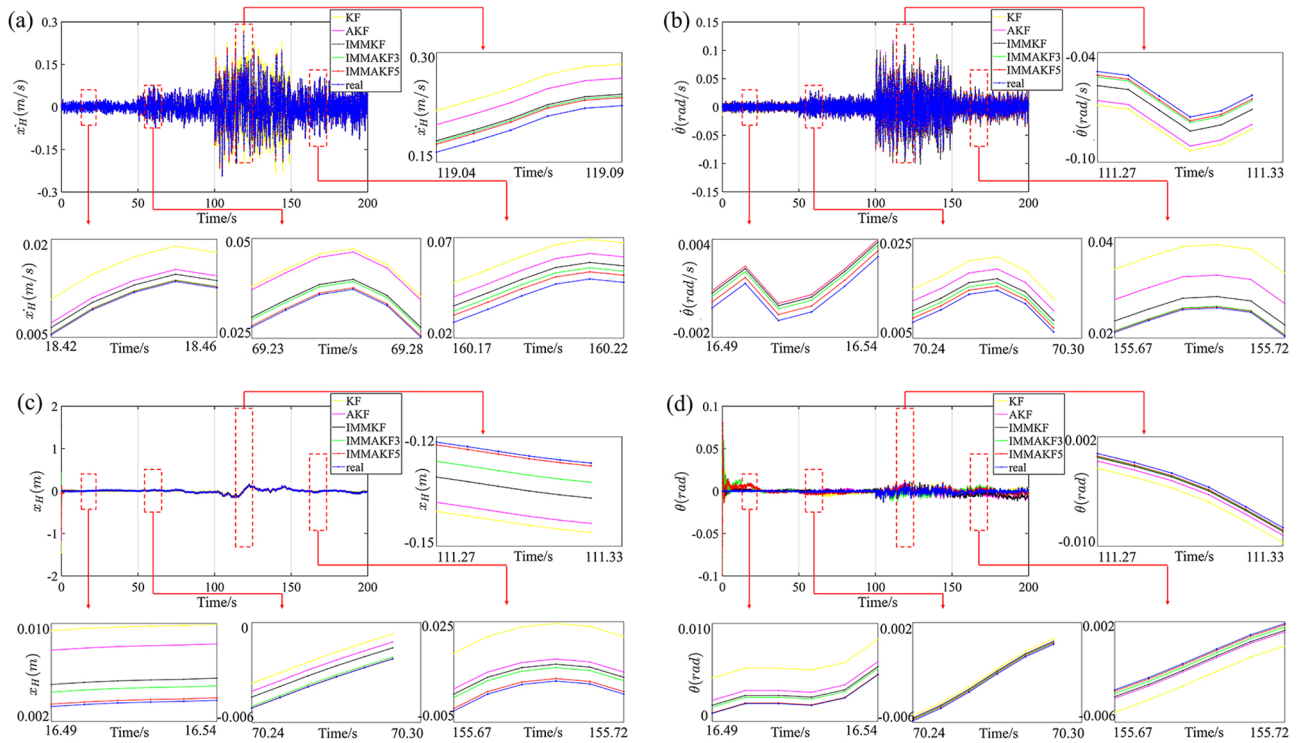
Figure 7. Model simulation and comparison results: (**a**) results of $\dot{x}_H$ (**b**) results of $\dot{\theta}$ (**c**) results of x_H (**d**) results of θ.

| Working Condition	Model	Simulation error/%									
		$\dot{x}_H$	$\dot{\theta}$	$\dot{x}_f$	$\dot{x}_r$	x_H	θ	x_f	x_r	q_f	q_r
Total	IMMAKF5	4.73	4.90	1.86	1.79	12.78	2.05	14.75	10.54	4.88	5.95
	IMMAKF3	5.06	4.91	1.90	1.83	15.46	2.21	15.01	10.82	5.05	6.17
	IMMKF	10.55	9.55	8.15	7.71	15.91	2.54	15.82	13.06	15.78	13.10
	AKF	10.96	9.58	8.24	7.80	17.28	3.26	18.55	16.30	19.23	16.44
	KF	11.88	8.96	9.01	8.70	20.21	3.31	20.39	19.20	20.31	19.52
Grade A	IMMAKF5	5.10	6.24	3.6	3.51	16.70	4.04	13.27	15.98	4.95	7.04
	IMMAKF3	6.08	6.23	3.91	3.63	17.54	4.06	14.39	20.54	5.87	7.92
	IMMKF	15.55	10.27	10.79	10.49	17.44	5.31	15.17	28.79	17.20	10.89
	AKF	15.97	10.06	10.80	10.45	18.72	5.67	19.52	28.75	17.84	16.78
	KF	17.26	10.04	10.84	10.55	25.09	9.12	20.58	29.57	24.74	20.25
Grade B	IMMAKF5	3.13	3.56	1.55	1.70	17.56	1.24	21.71	12.54	7.16	7.02
	IMMAKF3	3.16	3.91	1.66	1.89	21.60	1.72	22.65	14.44	7.53	8.19
	IMMKF	9.46	8.37	10.07	8.70	22.02	3.86	26.34	16.00	16.48	15.89
	AKF	10.66	8.74	10.48	8.73	23.08	3.41	27.74	19.61	16.97	19.90
	KF	12.50	9.63	11.36	9.64	23.43	4.15	28.69	20.01	21.42	20.45
Grade C	IMMAKF5	5.71	6.12	1.30	1.34	11.83	2.37	10.54	9.84	4.10	5.62
	IMMAKF3	5.90	6.35	1.31	1.35	15.01	2.43	11.84	11.61	4.14	6.56
	IMMKF	9.71	8.19	7.40	7.17	17.75	2.71	18.90	16.64	15.70	16.30
	AKF	9.16	8.15	7.36	7.02	17.98	2.75	18.96	18.39	18.68	18.36
	KF	10.17	8.97	7.91	7.92	18.88	4.51	19.49	18.82	26.53	19.20
Grade D	IMMAKF5	4.92	3.54	0.70	0.47	7.21	3.72	6.72	5.14	2.29	2.55
	IMMAKF3	5.14	3.55	0.71	0.50	8.74	4.46	10.58	5.16	3.52	2.81
	IMMKF	7.53	9.95	4.45	4.26	10.75	5.68	13.12	7.67	13.24	7.70
	AKF	6.27	9.58	4.45	4.11	12.29	7.14	19.46	9.66	20.16	20.91
	KF	10.89	7.94	6.17	5.88	14.41	8.20	19.81	17.74	23.77	16.87

Table 3. Comparison of simulation error.
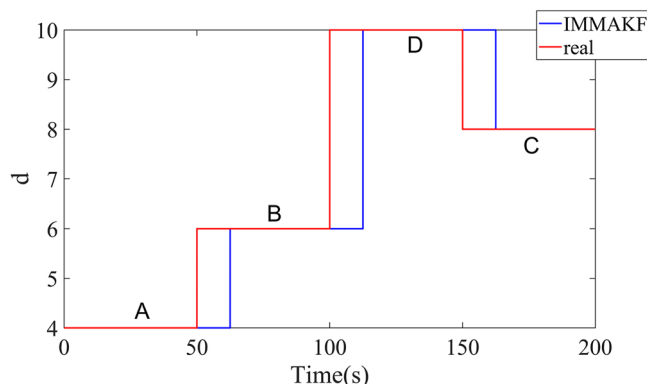
Figure 8. Road grade recognition results of IMMAKF.

During the simulation, the model interaction probability of IMMAKF3 and IMMAKF5 are shown as Fig. 9:

According to Fig. 9, during the model interaction process, IMMAKF always has a sub-model with the maximum probability, which is related to the current model state, i.e. the sub-model with the maximum interaction probability in IMMAKF algorithm is the current system state model, which can be used to estimate the current sprung mass. For Fig. 9, the n steps time window is used to estimate the sprung mass of the suspension model, and the accuracy of sprung mass estimation is shown in Table 4:

In Table 4, the larger the sampling step of the time window, the higher the model recognition accuracy, but the longer the model sampling time, and the longer the vehicle driving distance. When the sampling step is 500, the model has the highest accuracy and sampling time is also suitable, so 500 steps is considered as the optimal step size for sprung mass estimation.

According to Fig. 9 and Table 4, IMMAKF observers can not only ensure high estimation accuracy under variable working conditions, but also determine the sprung mass through analyzing model interaction probability.
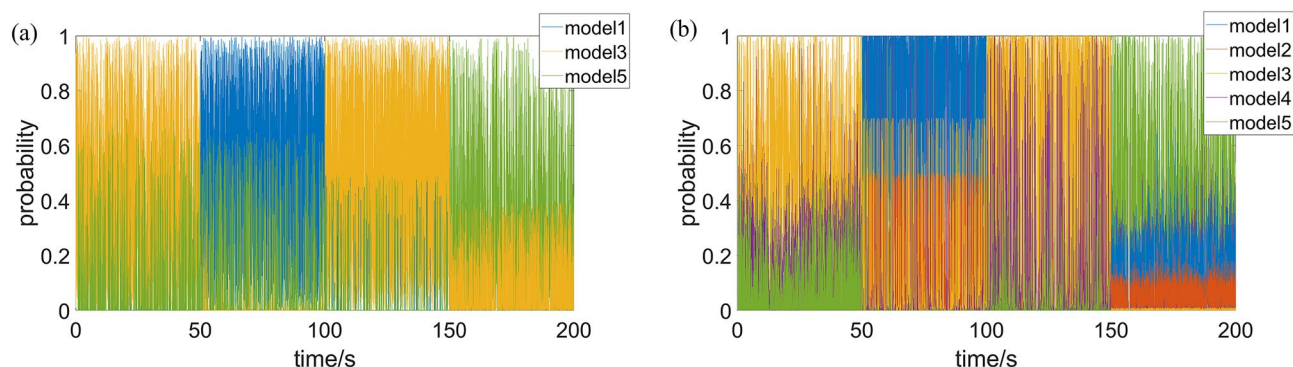
Figure 9. Model probability of IMMAKF. (**a**) Model probability of IMMAKF3 (**b**) Model probability of IMMAKF5. For model 1 to model 5, the sprung mass m_H is 300, 350, 400, 450, 500 kg, respectively.

Sampling step n	Model	Condition1	Condition2	Condition3	Condition4
1	IMMAKF3	68.10%	84.40%	89.60%	46.20%
	IMMAKF5	48.00%	66.80%	57.40%	40.10%
50	IMMAKF3	92.90%	100.00%	100.00%	55.50%
	IMMAKF5	69.80%	98.00%	91.80%	65.60%
100	IMMAKF3	97.90%	100.00%	100.00%	85.30%
	IMMAKF5	73.50%	100.00%	97.80%	77.50%
500	IMMAKF3	100.00%	100.00%	100.00%	100.00%
	IMMAKF5	100.00%	100.00%	100.00%	100.00%

Table 4. Sprung mass estimation accuracy of IMMAKF observers.

Experiment verification

The correctness of IMMAKF state observer is verified by the suspension experiment platform. The platform is shown in Fig. 10.

Since the platform is the quarter vehicle model, the suspension is used to simulate the front wheel. For the platform, the sprung mass is 2.45 kg, unsprung mass is 1 kg, the suspension stiffness is 900 N/m and the tire stiffness is 2500N/m. For the experiment, the road excitation is ISO A grade. The total experiment time is 10 s and the time interval is 0.02 s. The vehicle speed is 20 m/s. The experiment results of ordinary KF (i.e. 20 m/s vehicle speed, ISO C road and 2.45 kg sprung mass) and simulation results of IMMAKF5 are selected for comparison. To show the vibration effect (i.e. ride comfort and road handling stability), the passive suspension with damping of 7.5 Ns/m is used for verification (the passive suspension doesn't have observers, the results of passive suspension are obtained by sensors and calculated as comparison). The experiment results of $\dot{x}_{Hf}$ are shown in Fig. 11.

The simulation results comparison is shown in Table 5.

In Fig. 11, the experiment results of IMMAKF5 is close to real values and simulation values, which verifies the accuracy of the IMMAKF5. In Table 5, the experiment errors of IMMAKF5 is smaller than KF, which verifies the superiority of IMMAKF.

In Table 5, compared with the results of KF and passive suspension, the sprung mass acceleration of IMMAKF5 is improved by 14.64% and 62.73% respectively; the suspension deflection is improved by 11.43%
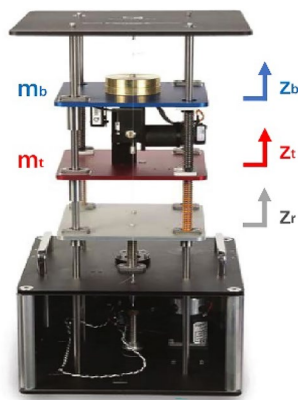

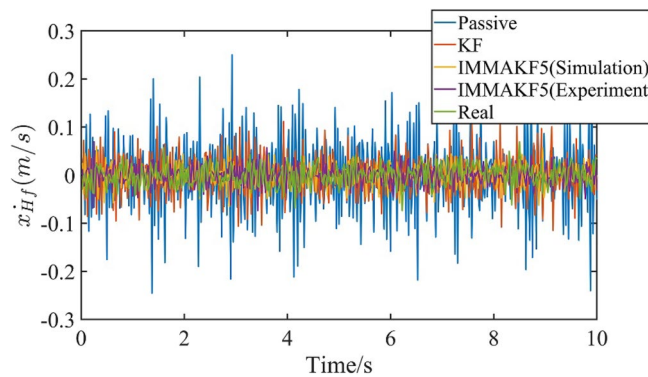**Figure 10.** Suspension experiment platform.

Figure 11. Suspension experiment results of $\dot{x}_{Hf}$.

Parameter type	Parameters	Model			
		IMMAKF5 (Simulation)	IMMAKF5 (Experiment)	KF	Passive
Observation error/%	$\dot{x}_{Hf}$	4.61	5.27	10.42	–
	$\dot{x}_f$	1.96	2.23	8.81	–
Vibration values	$\ddot{x}_{Hf}$	0.2862	0.2735	0.3204	0.7339
	$x_{Hf} - x_f$	0.0033	0.0031	0.0035	0.0121

Table 5. Simulation results comparison.

and 74.38% respectively, which verifies that the IMMAKF observer can improve the ride comfort and balance the handling stability of the vehicle.

Conclusions

In this paper, the IMMAKF suspension state observer is proposed for the state observation of the adaptive suspension model under variable working conditions (vehicle speed, road roughness grade and sprung mass). Firstly, the adaptive suspension controller is established. The LQR controller parameters under variable working conditions are optimized by NSGA-II algorithm. Referring to the optimal results, the fuzzy adaptive suspension controller is presented. The adaptive suspension can automatically change the optimal controller parameters by working conditions. Furthermore, the IMMAKF suspension state estimation theory is discussed in detail. Based on IMMKF and AKF, an IMMAKF suspension state observer is established, and the theoretical equations of the algorithm are derived. Lastly, the simulation and experiment results show that, compared with state observers of KF, AKF and IMMKF, the accuracy of the IMMAKF state observer is the highest and the ride comfort of IMMAKF is improved. Except for high estimation accuracy, the road roughness grade and sprung mass can be calculated by IMMAKF observer. Therefore, IMMAKF is effective for high suspension estimation accuracy and the adaptive control on complex conditions.

Note that the proposed method is a suspension state observer, which is established based on the typical working conditions, so the application of this proposed method is limited. The state estimation schema of full car suspension model under more complex working conditions such as the longitudinal vehicle speed with acceleration and the vehicle driving on slope roads, will be investigated in our future study. In addition, the road roughness grade identification by visual sensors will also be considered in the future study.

Data availability

All data generated or analysed during this study are included in this published article.

References

1. Nguyen, T. A. A novel approach with a fuzzy sliding mode proportional integral control algorithm tuned by fuzzy method (FSMPIF). *Sci. Rep.* **13**(1), 7327 (2023).
2. Mozaffari, A., Chenouri, S., Qin, Y. & Khajepour, A. Learning-based vehicle suspension controller design: A review of the state-of-the-art and future research potentials. *Etransportation.* **1**(2), 100024 (2019).
3. Nguyen, D. N. & Nguyen, T. A. Evaluate the stability of the vehicle when using the active suspension system with a hydraulic actuator controlled by the OSMC algorithm. *Sci. Rep.* **12**(1), 19364 (2022).
4. Soliman, A. M. A. & Kaldas, M. M. S. Semi-active suspension systems from research to mass-market—A review. *J. Low Freq. Noise Vib. Active Control* **40**(2), 1005–1023 (2021).
5. Jia, T. H., Pan, Y. N., Liang, H. J. & Lam, H. K. Event-based adaptive fixed-time fuzzy control for active vehicle suspension systems with time-varying displacement constraint. *IEEE Trans. Fuzzy Syst.* **30**(8), 2813–2821 (2022).
6. Chen, H., Liu, Y. J., Liu, L., Tong, S. C. & Gao, Z. W. Anti-saturation-based adaptive sliding-mode control for active suspension systems with time-varying vertical displacement and speed constraints. *IEEE Trans. Cybern.* **52**(7), 6244–6254 (2022).
7. Na, J. *et al.* Adaptive finite-time fuzzy control of nonlinear active suspension systems with input delay. *IEEE Trans. Cybern.* **50**(6), 2639–2650 (2020).
8. Li, H. Y., Zhang, Z. X., Yan, H. C. & Xie, X. P. Adaptive event-triggered fuzzy control for uncertain active suspension systems. *IEEE Trans. Cybern.* **49**(12), 4388–4397 (2019).
9. Taghavifar, H., Mardani, A., Hu, C. & Qin, Y. C. Adaptive robust nonlinear active suspension control using an observer-based modified sliding mode interval type-2 fuzzy neural network. *IEEE Trans. Intell. Vehicles* **5**(1), 53–62 (2020).
10. Liu, Y. J. *et al.* Adaptive neural network control for active suspension systems with time-varying vertical displacement and speed constraints. *IEEE Trans. Industr. Electron.* **66**(12), 9458–9466 (2019).
11. Wang, K. *et al.* Multidirectional motion coupling based extreme motion control of distributed drive autonomous vehicle. *Sci. Rep.* **12**(1), 13203 (2022).
12. Xia, X., Hashemi, E., Xiong, L. & Khajepour, A. Autonomous vehicle kinematics and dynamics synthesis for sideslip angle estimation based on consensus Kalman filter. *IEEE Trans. Control Syst. Technol.* **31**(1), 179–192 (2023).
13. Chen, F., Chen, S. R. & Ma, X. X. Analysis of hourly crash likelihood using unbalanced panel data mixed logit model and real-time driving environmental big data. *J. Safety Res.* **65**, 153–159 (2018).
14. Liu, Y. H. *et al.* An innovative information fusion method with adaptive Kalman filter for integrated INS/GPS navigation of autonomous vehicles. *Mech. Syst. Signal Process.* **100**, 605–616 (2018).
15. Theunissen, J. *et al.* Preview-based techniques for vehicle suspension control: A state-of-the-art review. *Annu. Rev. Control.* **51**, 206–235 (2021).
16. Theunissen, J. *et al.* Regionless explicit model predictive control of active suspension systems with preview. *IEEE Trans. Industr. Electron.* **67**(6), 4877–4888 (2020).
17. Wu, J. *et al.* Ride comfort optimization via speed planning and preview semi-active suspension control for autonomous vehicles on uneven roads. *IEEE Trans. Veh. Technol.* **69**(8), 8343–8355 (2020).
18. Zhang, Q. *et al.* Vehicle parameter identification and road roughness estimation using vehicle responses measured in field tests. *Measurement.* **199**, 111348 (2022).
19. Botshekan, M. *et al.* Smartphone-enabled road condition monitoring: from accelerations to road roughness and excess energy dissipation. *Proceed. R. Soc. Math. Phys. Eng. Sci.* **477**, 2246 (2021).
20. Qin, Y. C., Xiang, C. L., Wang, Z. F. & Dong, M. M. Road excitation classification for semi-active suspension system based on system response. *J. Vib. Control* **24**(13), 2732–2748 (2018).
21. Wang, R. C. *et al.* Vehicle attitude compensation control of magneto-rheological semi-active suspension based on state observer. *Proceed. Inst. Mech. Eng. Part D J. Automob. Eng.* **235**(14), 3299–3313 (2021).
22. Yin, X. Y., Li, Z. J. & Kolmanovsky, I. V. Distributed state estimation for linear systems with application to full-car active suspension systems. *IEEE Trans. Industr. Electron.* **68**(2), 1615–1625 (2021).
23. Ding, H.-L., Zhang, C., Gao, Y.-W. & Huang, J.-P. Extended Kalman filter algorithm for non-roughness and moving damage identification. *Sci. Rep.* **12**(1), 21958 (2022).

24. Khan, S. & Guivant, J. Fast nonlinear model predictive planner and control for an unmanned ground vehicle in the presence of disturbances and dynamic obstacles. *Sci. Rep.* **12**(1), 12135 (2022).
25. Yang, H., Kim, B. G., Oh, J. S. & Kim, G. W. Simultaneous estimation of vehicle mass and unknown road roughness based on adaptive extended Kalman filtering of suspension systems. *Electronics.* **11**(16), 2544 (2022).
26. Jin, X. J., Wang, Z. R., Yang, J. P., Xu, L. W. & Yin, G. D. Novel payload parameter sensitivity analysis on observation accuracy of lightweight electric vehicles. *Int. J. Automot. Technol.* **24**(5), 1313–1324 (2023).
27. Zhao, Z.K., Wang, C. W., Zhao, J. Q., Du, W., LQR force command planning-based sliding mode control for active suspension system. Proceed. Inst. Mech. Eng. Part I-J. Syst. Control Eng. (2023).
28. Kim, J., Lee, T., Kim, C. J. & Yi, K. Model predictive control of a semi-active suspension with a shift delay compensation using preview road information. *Control Eng. Pract.* **137**, 105584 (2023).
29. Batta, N. A. & Doscher, D. P. Model predictive control of a multi-mode suspension system using preview information and weight optimization. *J. Dyn. Syst. Meas. Control.* **145**(6), 065001 (2023).
30. Li, H. X., Liu, L. S., Zhen, L. X., Xu, Y. & Xie, X. Y. Rollover prediction and control strategy based on experiment for tractor semi-trailer fitted with hydraulically interconnected suspension. *Int. J. Control Automat. Syst.* **21**(1), 221–230 (2023).
31. Wang, Z. F. *et al.* Suspension system state estimation using adaptive Kalman filtering based on road classification. *Vehicle Syst. Dyn.* **55**(3), 371–398 (2017).
32. Wang, Z. F. *et al.* Vehicle system state estimation based on adaptive unscented Kalman filtering combing with road classification. *IEEE Access* **5**, 27786–27799 (2017).
33. Qu, Z., Liu, J., Li, Y., Yang, F. & Liu, J. Study on multi-mode switching control of intelligent suspension under full road section. *Processes.* **11**(6), 1776 (2023).
34. Zhang, Z. P. *et al.* State observers for suspension systems with interacting multiple model unscented Kalman filter subject to Markovian switching. *Int. J. Automot. Technol.* **22**(6), 1459–1473 (2021).
35. Liu, W., Wang, R., Ding, R., Meng, X. & Yang, L. On-line estimation of road profile in semi-active suspension based on unsprung mass acceleration. *Mech. Syst. Signal Process.* **135**, 106370 (2020).
36. Wang, R. C. *et al.* Switching control of semi-active suspension based on road profile estimation. *Vehicle Syst. Dyn.* **60**(6), 1972–1992 (2022).
37. Qin, Y. C. *et al.* A novel nonlinear road profile classification approach for controllable suspension system: Simulation and experimental validation. *Mech. Syst. Signal Process.* **125**, 79–98 (2019).
38. Kumar, V. & Rana, K. P. A novel fuzzy PID controller for nonlinear active suspension system with an electro-hydraulic actuator. *J. Braz. Soc. Mech. Sci. Eng.* **45**(4), 189 (2023).

Acknowledgements

Author contributions

Methodology, X.W. and W.S.; software, X.W.; validation, X.W., W.S. and Z.C.; writing—original draft preparation, X.W.; writing—review and editing, W.S.; funding acquisition, Z.C. and W.S. All authors have read and agreed to the published version of the manuscript.

Competing interests

The authors declare no competing interests.

Additional information

Supplementary Information The online version contains supplementary material available at https://doi.org/10.1038/s41598-023-49766-y.

Correspondence and requests for materials should be addressed to Z.C.

Reprints and permissions information is available at www.nature.com/reprints.

Publisher's note Springer Nature remains neutral with regard to jurisdictional claims in published maps and institutional affiliations.